First-Principles Study of Integer Quantum Hall Transitions in Mesoscopic Samples

Chenggang Zhou[1] and Mona Berciu[2]

[1] Department of Electrical Engineering, Princeton University, Princeton, New Jersey 08544, USA
[2] Department of Physics and Astronomy, University of British Columbia, Vancouver, BC V6T 1Z1, Canada

(Dated: April 14, 2024)

We perform first principles numerical simulations to investigate resistance fluctuations in mesoscopic samples, near the transition between consecutive Quantum Hall plateaus. We use six-terminal geometry and sample sizes similar to those of real devices. The Hall and longitudinal resistances extracted from the generalized Landauer formula reproduce all the experimental features uncovered recently. We then use a simple generalization of the Landauer-Buttiker model, based on the interplay between tunneling and chiral currents – the co-existing mechanisms for transport – to explain the three distinct types of fluctuations observed, and identify the central region as the critical region.

PACS numbers: 73.43.-f, 73.23.-b, 71.30.+h

Although the Integer Quantum Hall Effect (IQHE) is a generally well understood phenomenon, recent experiments on mesoscopic samples [1, 2] uncovered unexpected behavior in the seemingly noisy fluctuations of the Hall (R_H) and longitudinal (R_L) resistances. Previously, fluctuations in resistance had been observed in mesoscopic samples with a phase coherence length L larger than the sample size [3, 4, 5]; they are totally random, similar to universal conductance fluctuations [6]. By contrast, Peled et. al. find [1, 2] that the transition between the n^{th} and $(n+1)^{st}$ plateaus of the IQHE has three distinct regimes: (i) on the high-B side, both R_H and R_L have large but correlated fluctuations, such that $R_L + R_H = h/ne^2$; (ii) for intermediate B values, R_H and R_L continue to exhibit fluctuations, but their sum is no longer constant; and (iii) on the low-B side, $R_H = h/(n+1)e^2$ has no fluctuations, whereas R_L still does. Moreover, $R_L + R_H = R_{2t}$ holds for all B values [2]. Changing the sign of the magnetic field $B \to -B$ also has interesting consequences, as discussed later. For $n = 0$, regions (i) and (ii) are replaced by the transition to the insulating phase [1]. In this Letter, we explain the physics behind these observations in a unified theory, and analyze the implications for further experimental and theoretical study.

The relation $R_L + R_H = R_{2t}$ was first proposed by Streda et. al. [7], while the fluctuations of regime (iii) are reminiscent of Jain and Kivelson's theory on the resistance fluctuations of narrow samples [8]. These theories were questioned by Buttiker [9], based on formulas appropriate for a four-terminal geometry [10]. We take an approach similar to Buttiker's and use the multi-probe Landauer formula [10, 11] to calculate the resistances measured experimentally. However, we mirror the experiments by including six contacts in our model, namely the four voltage probes plus the source and the drain for the electrical current. Our model enables us to calculate both R_L and R_H, and reveals the very rich physics underlying the observation of the mesoscopic IQHE.

The response function of the system is a 6×6 conductance matrix $\hat{g}$, with which the current-voltage relation reads $I = \sum g V$. Here, I is the out-going current on the contact $= 1; \ldots; 6$ and V is the corresponding voltage. For a mesoscopic Hall bar, $\hat{g}$ characterizes the electrical response (since the system is inhomogeneous, local quantities such as the current density are not conceptually well-defined). $\hat{g}$ is calculated [11] by solving a multi-channel scattering problem: $g_{,\,6} = \frac{e^2}{h} \sum_{i,j} |t_{i,\,j}|^2$, where $t_{i,\,j}$ is the transmission amplitude from the j^{th} transverse channel of contact into the i^{th} transverse channel of contact for an electron at the Fermi energy E_F. Due to the absence of charge accumulation and to gauge invariance, $\sum_{\text{row}} g = \sum_{\text{column}} g = 0$. As a result, diagonal g_{row} are uniquely determined by $g = \sum_{\text{column}} g = \sum_{\text{row}} g$. This imposes a constraint on the off-diagonal elements of $\hat{g}$ for each .

Our model is sketched in Fig. 1(a). Six perfectly conducting contacts are linked to a 4 m 2 m sample which

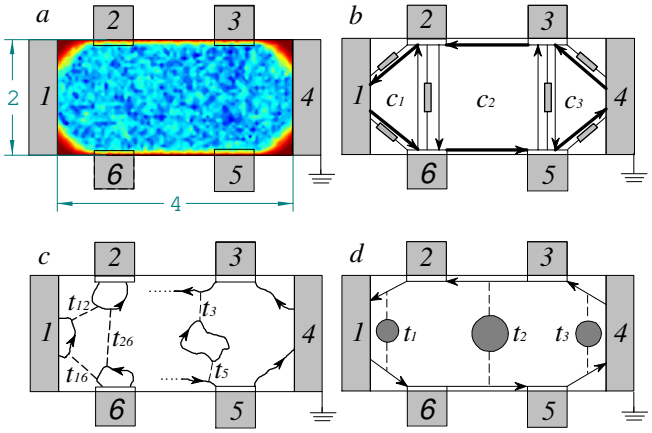

FIG. 1: (color online) (a) Typical potential $V_d + V_b$ of a 4 m 2 m sample. (b) Chiral (arrows) and tunneling (resistors) currents in our model. This direction of chiral currents corresponds to B entering the page. (c) Some semi-classical current distributions parameterized by our model. (d) Jain-Kivelson tunneling for high- . See text for further details.

has a disorder potential $V_d(r)$ and a background potential $V_b(r)$. $V_d(r)$ is a sum of random Gaussian scatterers generating elastic scattering inside the sample, while $V_b(r)$ confines the electrons to the sample and creates edge states. In our simulations, we include $L_x L_y B/\Phi_0 \approx 10^4$ states of the lowest Landau level (LLL), where $L_x L_y$ is the area of the sample and $\Phi_0 = h/e$ is the magnetic flux quantum. The sample Hamiltonian is a large, sparse matrix $H_{nm} = \langle n|V_b + V_d|m\rangle$. Contacts are modeled by ensembles of one-dimensional tight-binding chains attached to localized eigenstates on the corresponding edges of the sample. We have verified the multiprobe Landauer formula for our model using the linear response theory. This derivation and further modeling details will be reported elsewhere [12]. For a given magnetic field B, we numerically solve the scattering problem for different values of the Fermi energy and obtain $\hat{g}$. The filling factor ν is also a function of E_F, and thus we can find the dependence of the conductance matrix $\hat{g}$ on ν.

The resistances are then computed from $\hat{g}$. In the usual setup the current is injected in the source and extracted in the drain $I_1 = -I_4 = I$; $\hat{I}_{14} = [-I\ 0\ 0\ I\ 0\ 0]^T$. Without loss of generality we set $I = 1$ and $V_4 = 0$. The other five contact voltages are uniquely determined from $\hat{I}_{14} = \hat{g}\,\hat{V}$. We define two longitudinal resistances $R^L_{14;23} = (V_2 - V_3)/I = V_2 - V_3$, $R^L_{14;65} = V_6 - V_5$, and two Hall resistances $R^H_{14;62} = V_6 - V_2$, $R^H_{14;53} = V_5 - V_3$.

In Fig. 2, we plot representative matrix elements $g_{\alpha\beta}$ as a function of ν. For $\nu > 0.5$, we find $g_{\alpha,\alpha+1} \to e^2/h$ (if $\alpha = 6$, $\alpha+1 = 1$), with all other off-diagonal matrix elements vanishing. In other words, all electrons leaving contact $\alpha+1$ arrive at contact α. It follows that here

$$\hat{g} \to \hat{g}^{(0)} = \frac{e^2}{h}\,(\alpha\,\delta_{\alpha,\alpha+1} + \alpha+1\,\delta_{\alpha+1,\alpha}). \quad (1)$$

From $\hat{I}_{14} = \hat{g}^{(0)}\hat{V}$ we find $V_5 = V_6 = h/e^2$, $V_2 = V_3 = 0$, thus $R^H_{14;62} = R^H_{14;53} = h/e^2$, $R^L_{14;23} = R^L_{14;65} = 0$. This shows that the first quantized plateau is due to the chiral edge currents [shown as oriented thick lines in Fig. 1(b)], which become established for $\nu > 0.5$. Variations of $\hat{g}(\nu)$ from $\hat{g}^{(0)}$ give rise to fluctuations in the resistances. From Fig. 2 we also see that if $\nu < \nu_c$ (indicated by the vertical line), $g_{\alpha\beta} \approx g_{\beta\alpha}$ with high accuracy, i.e. $\hat{g}$ is symmetric. For $\nu > \nu_c$, $\hat{g}$ is no longer symmetric. The reasons for this behavior and its consequences are discussed later.

Using the conductance matrix $\hat{g}(\nu)$ plotted in Fig. 2, we now compute the values of the various resistances as a function of $0 < \nu < 1$. Fig. 3(a) shows a pair R_L and R_H. Three different regimes are clearly seen: for $\nu > 0.46$, $R_H = h/e^2$ and $R_L = 0$, corresponding to the first IQHE plateau. For $0.42 < \nu < 0.46$, R_L exhibits large fluctuations, however R_H is still well quantized. This is precisely the type of behavior observed in Ref. 1. For $\nu < 0.42$ the transition to the insulating phase occurs, and both resistances increase sharply. The fluctuations

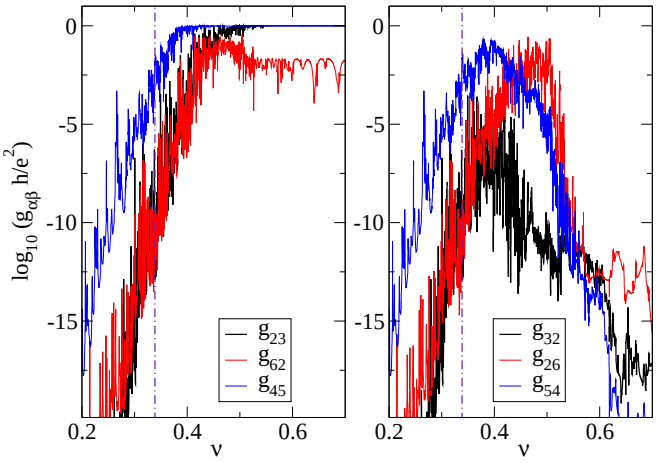

FIG. 2: (color online) Representative conductance matrix elements, in units of e^2/h, as a function of the filling factor ν. The left (right) panel shows g_{23}; g_{45} and g_{62}, respectively g_{32}, g_{54} and g_{26} characterizing transport in the (against the) direction of the edge currents. Results are almost identical on the left of the dot-dashed line, but different on its right.

are very large and narrow because the calculation is done at $T = 0$. At finite T, the peaks are smeared out.

The transition $1 < \nu < 2$ can also be simulated using the same $\hat{g}(\nu)$ matrix of the LLL. Similar to Ref. 13, we assume that the completely filled spin-up LLL contributes its background chiral edge current. As a result, we simply add $\hat{g}^{(0)} = \hat{g}(\nu = 1)$ of Eq. (1) to the values of $\hat{g}(\nu)$ describing the partially filled spin-down LLL. Although the two LLLs have different spins, the contacts mix electrons with both spins in equilibrium, justifying this addition. Resistivities $R^H_{14;62}$ and $R^L_{14;23}$ computed for $\hat{g}^{(0)} + \hat{g}(\nu)$ are shown in panel (b) of Fig. 3, whereas in panel (c) we plot their sum. The three regimes found experimentally [2, 14] are clearly observed. At low- ν (high-B), the fluctuations of R_H and R_L are correlated, $R_L + R_H = h/e^2$. At high- ν (low-B) $R_H = h/2e^2$ is quantized while R_L still exhibits strong fluctuations. In the intermediate regime, both R_H and R_L have strong, uncorrelated fluctuations. The other pair, $R^H_{14;53}$ and $R^L_{14;65}$, also exhibits the three regimes, although their detailed fluctuations are different from $R^H_{14;62}$ and $R^L_{14;23}$. From over 20 different simulations we found that the low- ν regime where $R_L + R_H = h/e^2$ is a very robust feature, although it is maintained up to different values of ν in different samples. The high- ν regime with fluctuations in R_L and quantized R_H is seen frequently. However, when strong direct tunneling occurs between the source or the drain and their nearby voltage probes, R_H also fluctuates. Such strong tunneling is an artifact of our simulation [15]. We suppress it by isolating the source and drain from nearby contacts with triangular potential barriers in the corners of the sample [see Fig. 1(a)]. Figure 3(c) also compares $R^L_{14;23} + R^H_{14;62} = R_{14;63}$ with

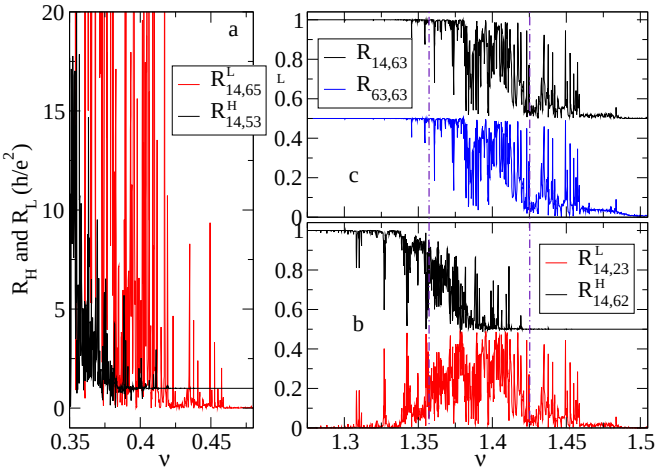

FIG. 3: (color online) R_L and R_H calculated from the conductance matrix displayed in Fig. 2, in units of $h=e^2$. (a) Transition from the insulator to the first IQHE plateau in the LLL. (b) Transition from the first to the second IQHE plateaus. (c) The sum $R_L + R_H$ of the resistances shown in (b), and R_{2t} 0:5$h=e^2$. Vertical lines indicate the boundaries of the critical region. See text for further details.

$R_{2t} = R_{63;63}$. [In the setup for measuring R_{2t}, the current is $\hat{I}_{63} =$ 0 0 1 0 0 1 ^{T}, and $R_{2t} = V_6$ V_3]. As found experimentally [2], the two curves are very similar.

So far, we have demonstrated that our numerical simulations recapture faithfully the experimental results. We now explain the underlying physics using a simple but very general model. For the given constraints and using logical induction, we find [12] that $\hat{g}$ can be decomposed as a sum over loops connecting contacts: $\hat{g} = \sum_p c(k_1; \ldots; k_n)\hat{\Gamma}(k_1; \ldots; k_n)$. Here, c are positive numbers and $\hat{\Gamma}(k_1; \ldots; k_n) = \hat{\Gamma}(k_1;k_2) + \ldots + \hat{\Gamma}(k_n;k_1)$, where $\hat{\Gamma}(a;b) = \frac{e^2}{h}$ $_a$ $_b$ $\frac{1}{2}$ $_a$ $_a$ $\frac{1}{2}$ $_b$ $_b$ contributes to a single off-diagonal element g_{ab}. A two-vertex loop $\hat{\Gamma}(a;b)$ describes a $h=e^2$ resistor between contacts a and b. Since $r(a;b) = r(a;b)$, these terms are the symmetric part to $\hat{g}$. The asymmetric part of $\hat{g}$ describes chiral currents, whose direction of flow is dictated by the sign of B. In particular, $\hat{\Gamma}(1;2;3;4;5;6) = \hat{g}^{(0)}$ of Eq. 1 describes the edge currents of a LL, but shorter chiral circuits may also develop at intermediate fillings .

At low , all states are localized and transport in the LL can only occur through tunneling. Consider the semiclassical case sketched on the left side of Fig. 1(c). Electrons can go from 2 to 1 either through direct tunneling (probability t_{12}), or they can tunnel to the localized state near contact 6 and from there back into 1, with probability $(1 \quad t_{12})t_{26}t_{16}(1 \quad t_{12})$. Electrons can make any number of loops before entering 1, the total sum being $p_{2!1} = \frac{h}{e^2}g_{12} = [t_{12} + t_{26}t_{16} \quad 2t_{12}t_{26}t_{16}]=(1 \quad t_{12}t_{16}t_{26})$. Similar arguments give $p_{1!2} = \frac{h}{e^2}g_{21} = [t_{12} \quad t_{26}t_{16} \quad t_{12}t_{16}]=(1 \quad t_{12}t_{16}t_{26})$. g_{16};g_{61};g_{26} and g_{62} are computed similarly. We define $r_{ab} = \min(p_{a!b};p_{b!a}) > 0$, and $c_{ab} = \max(p_{a!b};p_{b!a})$ $r_{ab} > 0$. We find $c_{12} = c_{26} = c_{61} = c = t_{12}t_{16} + t_{12}t_{26} + t_{16}t_{26} + O(t^3)$; and up to $O(t^2)$, r_{12} t_{12}, r_{16} t_{16} and r_{26} t_{26}. These processes contribute a total of $r_{12}\hat{\Gamma}(1;2) + r_{16}\hat{\Gamma}(1;6) + r_{26}\hat{\Gamma}(2;6) + c\hat{\Gamma}(1;2;6)$ to $\hat{g}$. The symmetric resistance terms, of order t, are due to direct tunneling between contacts, and at low they dominate the small chiral current, of order t^2. This explains why for $< _c$, $\hat{g}$ is symmetric with small off-diagonal components (see Fig. 2). At high enough , edge states connecting consecutive contacts appear. As already discussed, as ! 1, $\hat{g}$! $\hat{g}^{(0)} = \hat{\Gamma}(1;2;3;4;5;6)$. For intermediate , shorter chiral loops containing edge states can be established through tunneling, as sketched on the right side of Fig. 2(c). Assume that an electron leaving contact 3 can tunnel with probabilities t_3 and t_5 to and out of a localized state, to join the opposite edge current and enter 5. It follows that $p_{3!5} = \frac{h}{e^2}g_{53} = t_3t_5=[1 \quad (1 \quad t_3)(1 \quad t_5)]$, whereas $p_{5!3} = 0$ (no electron leaving 5 enters 3). Then $r_{35} = 0$ and the contribution to $\hat{g}$ is just $p_{3!5}\hat{\Gamma}(5;3)$. This term combines with parts of $\hat{\Gamma}(3;4)$ and $\hat{\Gamma}(4;5)$ to create a chiral current $c\hat{\Gamma}(3;4;5)$, where $c = p_{3!5}$. Physically, this represents the backscattered current of the Jain-Kivelson model [8].

In general, one has to sum over many types of competing processes, involving both tunneling and edge states, but $\hat{g}$ can always be decomposed into symmetric resistances plus chiral loops. Consider the general form $\hat{g} = n\hat{g}^{(0)} + r_{12}\hat{\Gamma}(1;2) + r_{16}\hat{\Gamma}(1;6) + r_{26}\hat{\Gamma}(2;6) + r_{34}\hat{\Gamma}(3;4) + r_{45}\hat{\Gamma}(4;5) + r_{35}\hat{\Gamma}(3;5) + c_0\hat{g}^{(0)} + c_1\hat{\Gamma}(1;2;6) + c_2\hat{\Gamma}(2;3;5;6) + c_3\hat{\Gamma}(3;4;5) + c_4\hat{\Gamma}(1;2;3;5;6) + c_5\hat{\Gamma}(2;3;4;5;6)$. The first term describes the contribution of the n completely filled lower LLs. All other terms describe transport in the LL hosting E_F [see Fig. 1(b)], with the restriction that there is no tunneling between the left and right sides of the sample. This is justified physically because tunneling between contacts far apart is vanishingly small. The largest such terms, r_{23} and r_{56}, are found to be less than 10^{-4} [see e.g. Fig. 2 , where $r_{23} = h=e^2$ $\min(g_{12};g_{32})$]. We solve both $\hat{I}_{14} = \hat{g}\hat{V}$ and $\hat{I}_{63} = \hat{g}\hat{V}^0$ and find the identity

$$R_{14;63} = R_{63;63} = \frac{h}{e^2}\frac{1}{n + c_0 + c_2 + c_4 + c_5}$$

Since $R_{63;63} = R_{2t}$, whereas $R_{14;63} = R^H_{14;62} + R^L_{14;23} = R^L_{14;65} + R^H_{14;53}$, this means that $R_{2t} = R_H + R_L$ irrespective of the value of the 12 parameters. In other words, this identity is obeyed for all , in agreement with Fig. 3(c). (Adding r_{23} and r_{56} terms leads to perturbationally small corrections [12]). Here $n + c_0 + c_2 + c_4 + c_5$ is the total chiral current flowing along the 6 ! 5 and 3 ! 2 edges. In particular, at low chiral currents in the LL hosting E_F are vanishingly small $c_0 = c_2 = c_4 = c_5 = 0$ (there are no edge states established yet, and pure tunneling contributions are of order t^2, as already discussed. Below $_c$, all $t < 10^{-4}$, see Fig. 2). It follows that here $R_L + R_H = h=ne^2$, explaining the perfect correlations in

the pattern fluctuations at low- of the two resistances, observed both experimentally and numerically.

The high- regime with quantized R_H and fluctuating R_L can also be understood easily. As already discussed, transport in the LL hosting E_F is dominated here by the edge states; tunneling between opposite edge states (facilitated by localized states inside the sample) creates backscattered currents, as in the Jain-Kivelson model [8]. We sketch this situation in Fig. 1(d), where t_1, t_2 respectively t_3 include all possible tunneling processes leading to backscattering on the corresponding pairs of edge states. Reading the various probabilities of Fig. 1(d), we find that $\hat{g} = n\hat{g}^{(0)} + (1 - t_1 - t_2 - t_3)\hat{g}^{(0)} + t_2[\hat{r}(1;2;6) + \hat{r}(3;4;5)] + t_3\hat{r}(1;2;3;5;6) + t_1\hat{r}(2;3;4;5;6)$. The first term represents the contribution of the lower n completely filled LLs, the others are the forward and the backscattered chiral currents in the LL hosting E_F. $\hat{I}_{14} = \hat{g}\,\hat{V}$ is trivial to solve. We find $R^H_{14;62} = R^H_{14;53} = h/(n+1)e^2$, i. e. the Hall resistances are precisely quantized, whereas $R^L_{14;23} = R^L_{14;65} = [h/(n+1)e^2]\,t_2/(n+1-t_2)$. Since t_2 has a strong resonant dependence on E_F (or), it follows that R_L fluctuates strongly. In particular, if $n = 0$ (transition inside spin-up LLL), R_L can be arbitrarily large when $t_2 \to 1$, whereas in higher LLs the amplitude of fluctuations in R_L is $h/(n+1)e^2$ or less, as observed both experimentally and in our simulations.

If B changes sign, we have verified that the identity $\hat{g}(-B) = [\hat{g}(B)]^T$ holds [11]. The reason is that time-reversal symmetric tunneling is not affected by this sign change, while the flow of the chiral currents is reversed. The model mirrors itself with respect to the horizontal axis if B changes sign, see Fig. 1. The solutions of $\hat{I}_{14} = \hat{g}(-B)\,\hat{V}$ are then related to the solutions of $\hat{I}_{14} = \hat{g}(B)\,\hat{V}$ by $v_2 = V_6$, $v_3 = V_5$, $v_5 = V_3$ and $v_6 = V_2$, provided that the same index exchanges $2 \leftrightarrow 6$, $3 \leftrightarrow 5$, are performed for all r_{ab}. Terms not invariant under this transformation are r_{12}, r_{16}, r_{43}, r_{45}, r_{23} and r_{56}. As already discussed, the last two terms are vanishingly small. In the experimental setup, the first four terms are also very small, due to the long distance between source and drain, and their nearby contacts [15]. The dominant terms r_{26} and r_{35} are invariant under the index exchange. It follows then that $R^L_{14;23}(B) = R^L_{14;65}(-B)$ and vice versa, i. e. with good accuracy, the fluctuation pattern of one R_L mirrors that of the other R_L when $B \to -B$. This symmetry has indeed been observed experimentally, with small violations at low- [14] due to perturbative corrections from the non-invariant tunneling contributions $r_{12} - r_{16}$ and $r_{43} - r_{45}$.

We now summarize our understanding of the various results of IQHE measurements on mesoscopic samples. Similar to experiments, we find that the transition in higher LLs is naturally divided in three regimes. At low- , the LL hosting E_F is insulating and there are no edge states connecting the left and right sides of the sample. If tunneling between left and right sides is also small, we find that the fluctuations of pairs of resistances are correlated with excellent accuracy, $R_H + R_L = h/ne^2$. This condition is obeyed if the typical size of the wave-function (localization length) is less than the distance between contacts 2 and 3. When the localization length becomes comparable to this distance, an edge state is established and the correlation between R_L and R_H is lost. On the high- side the edge states are established, but localized states inside the sample can help electrons tunnel between opposite edges, leading to back-scattering like the Jain-Kivelson model. In this case, we showed that R_L fluctuates while R_H is quantized. Tunneling between opposite edges is likely only if the typical size of the wave-functions is slightly shorter than the distance between opposite edges. It is then apparent that the central regime in Figs. 3 (b) and (c) corresponds to the so-called "critical region", where the typical size of the electron wave-function is larger than the sample size (distance between contacts 2 and 3, at low- , or between 2 and 6 at high-). In these mesoscopic samples, the voltage probes act as markers on a ruler, measuring the localization length of the wave-functions at the Fermi energy. To our knowledge, this is the first time when the boundaries of the critical region are pinpointed experimentally. This opens up exciting possibilities for experimentally testing the predictions of the localization theory.

To conclude, we used both first-principles simulations and a simple model to explain the phenomenology of the mesoscopic IQHE, for six-terminal geometry. We identified tunneling and chiral currents as coexisting mechanisms for charge transport in mesoscopic samples, and argued that the boundaries between the three distinct regimes mark the critical region.

This research was supported by NSERC and NSF DMR-0213706. We thank Y. Chen, R. Fisch, R. N. Bhatt and D. Shahar for helpful discussions.

[1] E. Peled et. al., Phys. Rev. Lett. 90, 246802 (2003).
[2] E. Peled et. al., to appear in Phys. Rev. Lett.; cond-mat/0307423.
[3] A. M. Chang et. al., Solid State Commun. 76, 769 (1988); G. Timp et. al., Phys. Rev. Lett. 59, 732 (1987).
[4] J. A. Simmons et. al., Phys. Rev. Lett. 63, 1731 (1989).
[5] D. H. Cobden et. al., Phys. Rev. Lett. 82, 4695 (1999).
[6] S. Cho and M. P. A. Fisher, Phys. Rev. B, 55, 1637 (1997).
[7] P. Streda et. al., Phys. Rev. Lett. 59, 1973 (1987).
[8] J. K. Jain and S. A. Kivelson, Phys. Rev. Lett. 60, 1542 (1988).
[9] M. Buttiker, Phys. Rev. Lett. 62, 229 (1989).
[10] M. Buttiker, Phys. Rev. Lett. 57, 1761 (1986); Phys. Rev. B 38, 9375 (1988).
[11] H. U. Baranger and A. D. Stone, Phys. Rev. B 40, 8169 (1989).
[12] C. Zhou and M. Berciu, in preparation.

[13] D. Shahar et. al., Phys. Rev. Lett. 79, 479 (1997).
[14] Y. Chen and D. Shahar (private communication).
[15] We use short samples (4 m 2 m) in order to save CPU time by decreasing the number of states in the LLL; experimental devices are much longer (24 m 2 m).